2023

APPLICATION OF SECONDARY CONTROL FOR MICROGRID RESILIENCE

Alexis R. Charpentier
University of Rhode Island, acharpentier20@uri.edu

APPLICATION OF SECONDARY CONTROL FOR MICROGRID RESILIENCE

BY

ALEXIS R. CHARPENTIER

A THESIS SUBMITTED IN PARTIAL FULFILLMENT OF THE

REQUIREMENTS FOR THE DEGREE OF

MASTER OF SCIENCE

IN

ELECTRICAL ENGINEERING

UNIVERSITY OF RHODE ISLAND

2023

MASTER OF SCIENCE THESIS

OF

ALEXIS R. CHARPENTIER

APPROVED:

Thesis Committee:

Major Professor Haibo He

Yan Sun

Manbir Singh Sodhi

Brenton DeBoef
DEAN OF THE GRADUATE SCHOOL

UNIVERSITY OF RHODE ISLAND

2023

ABSTRACT

Microgrid development has increased over the past years to account for the growing need for renewable energy sources. Conventional power generation methods such as large centralized power plants produce CO_2 emissions and have a negative impact on the environment. Extreme weather events as a result of climate change increase energy demand and risks to infrastructure and are capable of threatening generation capability. Further, electricity demand is increasing with more electric applications emerging such as electric vehicles and heating and cooling systems. Microgrids are a solution to integrate renewable energy sources to combat the negative effects the conventional methods have on the environment and the continuously increasing electricity demands. They may operate in grid connected or islanded mode depending on the application. In islanded operation, the microgrid must adopt control methods to regulate voltage and frequency and to balance power. Past research has indicated that distributed control methods improve system reliability over centralized control methods which require complex communication networks and are vulnerable to single point failure. Distributed control structures require a communication network between neighboring distributed generators (DGs) resulting in cyber vulnerabilities. To reduce susceptibility to disturbances and threats in the system, secondary control strategies are required to maintain voltage and frequency stability and active power sharing for balanced generation and load.

The resilience of a microgrid is supported by different secondary control strategies. In this thesis, I will review secondary control methods from literature and further analyze the performance of one model. Threats on the cyber layer, or communication network, of a microgrid may include denial of service or false data injection attacks. These threats will be modelled and implemented in a microgrid

to examine the control algorithm's performance in the presence of such a threat. Performance of the microgrid will also be analyzed under communication topology changes to further investigate secondary control for microgrid resilience.

ACKNOWLEDGMENTS

I would like to express deepest gratitude to my research advisor, Dr. Haibo He. His enthusiasm, engagement, and continuous guidance through this process has not only made this master thesis research possible but also enjoyable. Throughout my time as a research assistant, Dr. Yan Sun, my first committee member, has shown great interest and support for my research, which I am grateful for. I would like to thank my second committee member, Dr. Manbir Sodhi, for taking me in to work in his lab during my undergraduate degree, encouraging me in my academic career, and supporting me throughout my experience as a master's student.

I would also like to thank everyone in the Computational Intelligence and Self-Adaptive Systems (CISA) Laboratory for their support and collaboration, with extended regards to Zhenhua Wang for his patience and guidance in my research.

Finally, my parents Tom and Diana deserve the most special appreciation for enduring their own hardships to give me the opportunity to pursue this degree. I owe my academic career and all future endeavours to them and their unwavering support. They motivated me my whole life to pursue something I would enjoy and take pride in.

During my M.S. study, my research have been partially supported by the Office of Naval Research (ONR) under N00014-18-1-2396 and N00014-20-C-1096. Any opinions, findings, and conclusions or recommendations expressed in this material are those of the author and do not necessarily reflect the views of the Office of Naval Research. I gratefully acknowledge the support from ONR for my research.

TABLE OF CONTENTS

Page

LIST OF FIGURES

LIST OF TABLES

Table **Page**

CHAPTER 1

Introduction

The driving factor for climate change and global warming is burning fossil fuels to generate power, resulting in increased CO_2 emissions [5]. Climate change threatens the reliability of the electric grid as extreme weather is becoming increasingly common. Extreme heat, drought, wildfires, and hurricanes are all predicted to be higher than average and at above-normal risk. Extreme heat increases energy demand for cooling which strains the current infrastructure, drought limits generation at plants where water is used for cooling, and wildfires and hurricanes can damage or destroy existing infrastructure [6]. These threats not only increase demand and the likelihood of risks to infrastructure, but also have the potential to lower generation capability.

Coal, natural gas, oil, renewable, and nuclear energy all contribute to producing electricity, which accounted for one-third of energy related CO_2 emissions in 2021 [7]. Electricity demand is further increasing, driven by the expansion of end uses including electric vehicles, heat pumps, space cooling applications, etc.. In response to this increasing demand, new power capacity is set to be comprised of primarily solar PV and wind. The need to transition to clean and reliable energy from the traditional generation sources is essential to reduce the threats of climate change and to relieve the grid of the added demand and risk of failure.

Integration of renewable energy sources can improve worsening climate conditions and their negative impacts on the reliability of the power grid. The share of renewable sources in the electricity generation mix was 29% in 2020 [5] and renewable energy generation continues to increase. The microgrid is the key component to integrate renewable energy sources such as solar, wind, and hydro power. A

microgrid is a system used to connect the low voltage generation sources to loads and energy storage devices. The distributed generators (DGs) are connected to the grid using voltage source inverters (VSI) as described in [8]. The deployment of these low-voltage systems are focused on peak load reduction, renewable energy integration, and reliability in the system and at critical facilities [9].

Microgrids can operate in both grid-connected and islanded modes. When in grid-connected mode, the microgrid is connected to a larger power system which autonomously manages it by providing voltage/frequency support and active/reactive power balance between generation and demand [8, 10]. Microgrids may also operate in islanded mode which can be pre-planned or forced if there is a fault in the primary system. In islanded mode, a hierarchical control structure is adopted to ensure voltage and frequency stability and regulation as well as balanced power sharing between DGs. Hierarchical control involves inner control loops, primary control, and secondary control. The primary control is responsible for maintaining active and reactive power sharing and stabilizing voltage and frequency values. Stabilizing voltage and frequency, however, does not ensure they are regulated to their nominal values, so secondary control is required here to eliminate voltage and frequency deviations cause by primary control. Distributed secondary control improves resilience and avoids single point failure compared to centralized control which requires a complex communication-dense network. The distributed method employs a sparse communication network where only neighboring DGs exchange information and control signals are computed locally [11]. This necessary communication network in microgrids classifies them as a cyber-physical system which makes them vulnerable to cyber threats [12, 13], and jeopardizes their overall resilience.

Communication links in microgrids make them at risk for threats in the cyber

layer. Under threat, the control algorithm should continue to stabilize voltage and frequency and achieve power sharing in the microgrid. Cyber threats on microgrids may include denial of service (DOS), false data injection (FDI) [4, 12, 14, 15], and communication disruption. The denial of service attack is designed to prevent communication between DGs. Thus, frequency, power, and voltage information exchanged in the cyber layer are blocked and the targeted DGs will not receive that information. False data injection affects the integrity of information being communicated in the cyber layer by adding an attack signal to the communicated data. Communication disruptions are modelled in this thesis by altering the communication directed graph, or digraph that defines which DGs exchange information with each other in a distributed control structure.

Resilience of a microgrid can be compared under varying circumstances when secondary control is applied. This thesis aims to analyze secondary control for maintaining frequency and voltage stability and active power sharing against threat models and communication disruption between DGs. A distributed microgrid consisting of five DGs and five loads will be modelled. In this thesis, I will implement a distributed secondary control algorithm and analyze the frequency, active power, and voltage characteristics of each DG under the threat scenarios: DOS, FDI, and communication disruption. Examinations of these parameters will focus on oscillations and convergence time in response to the modelled scenarios.

This thesis contains six chapters which are organized as follows: Chapter 1 introduces the challenges surrounding the power system's impact on the environment and solutions found by using microgrids to integrate renewable energy sources. Vulnerabilities in microgrids as a cyber physical system are explained, but there are control methods which should result in a resilient microgrid. Chapter 2 then reviews the hierarchical control methods of microgrids from literature.

First, there is the widely accepted droop control for the primary control layer responsible for maintaining frequency and voltage stability and power sharing. Then, literature proposing secondary control methods that are responsible for regulating frequency and voltage deviations is reviewed and discussed. Chapter 3 defines the microgrid model used in this thesis characterized by the physical configuration of the microgrid, the local controllers, and the communication topology. Chapter 4 contains the analysis which characterize the control methods and cyber physical threats to the system. Simulation specifications and parameters are detailed in Chapter 5. Then, the results are provided along with a review of the performance of the secondary control method under the threats to the system. Finally, Chapter 6 concludes this thesis by summarizing the previous chapters and presents possible future work.

CHAPTER 2

Literary Review

With the recent urge to reduce CO_2 emissions due to worsening climate change, renewable energy sources are changing the power grid. Integration of these resources as power generation can be done using microgrids. In normal operation, the microgrid is connected to the main power grid however, in the case of a disturbance or other applications such as rural setting or automotive, the microgrid will enter islanded operation. When operating in islanded mode, the microgrid may lose stability due to a mismatch in power generation and consumption [16] and needs a control structure to operate autonomously. Thus, primary control is responsible for active and reactive power sharing and stabilizing voltage and frequency values locally. Frequency and voltage droops impact stability thus frequency-power and voltage-reactive power droop methods are used to balance power and regulate voltage and frequency in islanded microgrids [17]. Primary control may cause deviations from nominal values, thus secondary control is required to regulate voltage and frequency. The results from secondary control are used as inputs to the primary controller to compensate these deviations [3].

2.1 Primary Control

Inner control loops include voltage and current controllers and droop controllers where reference voltage and frequency values are calculated based on active and reactive power. The reference input to the local voltage controller is calculated by the droop controller. In references [3, 18, 19, 20], the droop control equations are adopted to specify the frequency and voltage magnitude. The characteristics

explicitly defined in [3] are as follows:

$$\omega_i = \omega_{ni} - m_i P_i$$

$$v^*_{o,magi} = V_{ni} - n_i Q_i$$

where ω_{ni} and V_{ni} are the network frequency and voltage references set in the secondary control layer, ω_i and $v^*_{o,magi}$ are the angular frequency of the DG and reference voltage value for the inner voltage control loop, P_i and Q_i are the measured active and reactive power injections, and m_i and n_i are the respective $P-\omega$ and $Q-E$ droop coefficients.

In [10, 11, 21], a correction term is presented to account for secondary control in the droop controller as follows:

$$\omega_i = \omega_{ref} - m_i P_i + u_{\omega,i}$$

$$v_i = v_{ref} - n_i Q_i + u_{v,i}$$

These additional u_i terms are to account for secondary control equations as ω_{ref} and v_{ref} here are the frequency and voltage set points rather than the reference values from the secondary control layer. Ultimately, both forms of the droop controllers achieve the same result.

To achieve system stability, the following must be true: frequency and voltage should be regulated to nominal values such that ω_i reaches ω_{ref} and v_i reaches v_{ref} in finite time. Active/reactive power sharing should be maintained such that $P_i/P_j = m_i/m_j$ and $Q_i/Q_j = n_i/n_j, \forall i, j \in N$.

2.2 Secondary Control

The droop equations take references from the secondary control to stabilize frequency and voltage values, although this may cause deviations from nominal values, and are responsible for accurate power sharing. Thus, secondary control is

required to regulate frequency and voltage to their nominal values. As described in reference [19], after any load or generation change, the secondary control will drive the deviations of frequency and voltage to zero. The output frequency and voltage are measured at each DG and compared with their respective reference values. The resulting control signal is sent back to each DG to restore the frequency and voltage to their nominal values. Fast convergence time, performance, and robustness are factors desirable when designing a control algorithm for a microgrid according to [4]. Here I will discuss different secondary control techniques for frequency and voltage restoration found in literature.

2.2.1 Centralized Control

Centralized control is the traditional architecture for secondary control. A central controller is described in [1, 22] where a remote sensor measures frequency and voltage values in the microgrid which are sent to the microgrid central controller

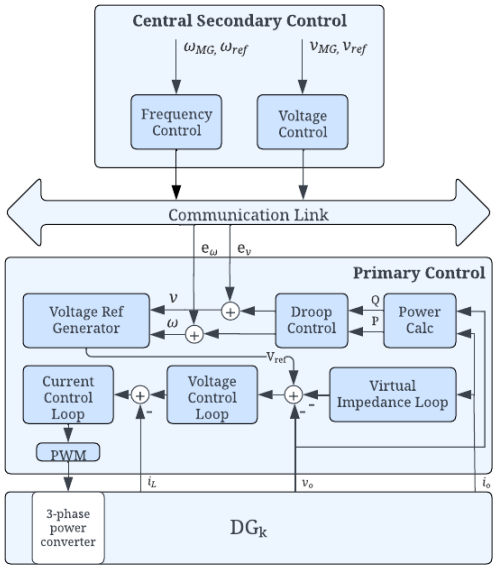

Figure 1. Block diagram of the secondary central control structure [1]

(MGCC). The measured values sent to the MGCC are compared with reference frequency and voltage values. then processed through a proportional integral (PI) controller to produce the control signal which is sent to the primary controller, depicted in Figure 1. This only requires unidirectional communication from the sensor to the MGCC and from the MGCC to each DG.

The central control structure defined in [16] compares the microgrid's frequency and each DG's terminal voltage to the reference frequency, ω_{ref}, and reference voltage, v_{ref}, respectively. The error signals $e_{\omega i}$ and e_{vi} are calculated and sent to the DG's primary controller [16].

$$e_{\omega i} = (\omega_{ref} - \omega_i) + K_{I\omega} \int (\omega_{ref} - \omega_i) dt$$

$$e_{vi} = K_{PE}(v_{ref} - v_i) + K_{IE} \int (v_{ref} - v_i) dt$$

where $K_{P\omega}$, $K_{I\omega}$, K_{PE}, and K_{IE} are PI control parameters. While the central controller performs well, it is vulnerable to single-point failure since all DG's communicate through and rely on the MGCC. Therefore, a more resilient and scalable distributed control architecture has been studied.

2.2.2 Distributed Control

Distributed secondary control of islanded AC microgrids relies on data exchange between neighboring DGs to synchronize frequency and voltage to their reference values. There are different algorithms that can be used to implement distributed control for microgrids. For instance, reference [3] proposes a distributed cooperative control algorithm for secondary voltage control where each DG only communicates with its neighbor. This algorithm chooses V_{ni}, the primary control input, so that the output voltage magnitude of the DG, $v^*_{o,magi}$, synchronizes to the reference voltage, v_{ref}. The local neighborhood tracking error aims to drive the output voltage of the DG to the reference value by taking the sum of the differences

between the output voltage of the DG and its neighbors, which are defined by an adjacency matrix, and added to the difference between the output voltage of the DG and the reference values weighted by the pinning gain which is only nonzero for one DG [3].

$$\mathbf{e}_i = \sum_{j \in N_i} a_{ij}(\mathbf{y}_i - \mathbf{y}_j) + g_i(\mathbf{y}_i - \mathbf{y}_0)$$

where a_{ij} denotes elements of the adjacency matrix, defining which DGs have communication with each other and g_i denotes the pinning gain that determines which DG has access to the reference value. The q component of the output voltage of the DG, $v^*_{o,magi}$, is 0, so $\mathbf{y}_i$, $\mathbf{y}_j$ and $\mathbf{y}_0$ are defined as $\begin{bmatrix} v_{odi} \\ \dot{v}_{odi} \end{bmatrix}$, $\begin{bmatrix} v_{odj} \\ \dot{v}_{odj} \end{bmatrix}$ and $\begin{bmatrix} v_{ref} \\ 0 \end{bmatrix}$, respectively.

A secondary voltage control algorithm is presented in [2] where the pinning gain determines the one DG that has access to the reference voltage value and where $\begin{bmatrix} y_{i1} \\ y_{i1,2} \end{bmatrix} = \begin{bmatrix} v_{odi} \\ \dot{v}_{odi} \end{bmatrix}$. The voltage control structure is described in Figure 2, similar to that presented in [3].

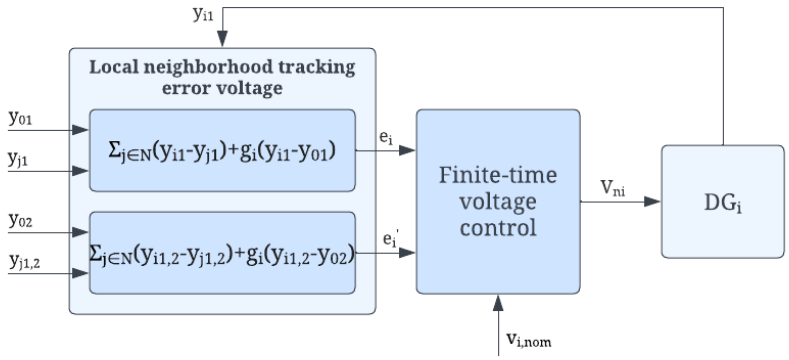

Figure 2. Block diagram of the distributed robust finite-time secondary voltage control proposed in [2]

It is noted that in accurate voltage control, a trade-off must be made with the accuracy of reactive power sharing due to the line impedance effect. Reference [2] also proposes a frequency control algorithm, constructed analogously to the voltage

control. The finite time frequency control signal, e_{ω_i}, takes the information from the i^{th} DG and compares it to the information from the neighboring DGs. The angular frequency of the DG is synchronized to its nominal frequency, ω_{ref}, in the following way [2]:

$$e_{\omega i} = -k_\omega \left(\sum_{j \in N_i} sig(\omega_i - \omega_j)^{\alpha_\omega} + g_i sig(\omega_i - \omega_{ref})^{\alpha_\omega} \right) - k_\omega \sum_{j \in N_i} sig(m_i P_i - m_j P_j)^{\alpha_\omega}$$

where k_ω and α_ω are the control parameters. The primary control input ω_{ni} can be defined as $\omega_{ni} = \int e_{\omega_i}, i = 1, 2, ..., N$.

Bounded varying time delays are addressed in [11] where an event-triggered controller is designed effectively solving the frequency restoration problem with time delays and reducing the communication burden of the microgrid. This algorithm also has a pinning gain which determines whether the i^{th} DG has access to the nominal frequency. The frequency and power allocation control signals, $e_{\omega i}$ and e_{Pi}, determine the secondary control compensation term to the droop control, $u_{\omega,i}$, as follows [11]:

$$u_{\omega,i} = \int e_{\omega i} + e_{Pi} dt$$

where

$$e_{\omega i} = g_\omega \sum_{j \in N} \left(\omega_i(t^i_{\omega,k} h) - \omega_j(t^j_{\omega,k'} h) \right) + b_i g_\omega (\omega_i(t^i_{\omega,k} h) - \omega_n)$$

$$e_{Pi} = g_P \sum_{j \in N} \left(k_{Pi} P_i(t^i_{P,k} h) - k_{Pj} P_j(t^j_{P,k'} h) \right)$$

The event-triggered sequence $(t^i_{\omega,k} h)$ is generated by dynamic event triggered mechanisms.

A consensus-based distributed secondary control is proposed in [21] that restores the average bus voltage to the rated value at steady state. The PI consensus algorithm regulates the compensation term $u_{v,i}$ to satisfy the voltage restoration and reactive power sharing without being affected by communication delays. It is

designed as follows [21]:

$$\dot{u}_{v,i} = \sum_{j \in N} a_q(n_j Q_j - n_i Q_i) - \sum_{j \in N} b_q(\zeta_{vj} - \zeta_{vi}) - g_q(u_{v,i} - n_i Q_i)$$

$$\dot{\zeta}_{vi} = -\sum_{j \in N} b_q(n_j Q_j - n_i Q_i)$$

This algorithm combines reactive power sharing and voltage recovery, simplifying the control structure and negating the need for a leader to supply the reference. The PI consensus algorithm is also designed to restore frequency and realize active power sharing. In contrast to the voltage control algorithm, the frequency compensation term $u_{\omega i}$ should be equal in each DG, so the necessary equation to satisfy is simply $u_{\omega i} - m_i P_i = 0$. The resulting control algorithm compares the compensation terms as follows [21]:

$$\dot{u}_{\omega,i} = \sum_{j \in N} a_p(u_{\omega,j} - u_{\omega,i}) - \sum_{j \in N} b_p(\zeta_{\omega j} - \zeta_{\omega i}) - g_p(u_{\omega,i} - m_i P_i)$$

$$\dot{\zeta}_{\omega i} = -\sum_{j \in N} b_p(u_{\omega,j} - u_{\omega,i})$$

The distributed secondary control algorithm in [1] proposes each DG collects frequency, voltage amplitude, and reactive power measurements from DG units defined by the communication system, averages them, and sends the resulting control signal to the primary control algorithm. The averaging frequency control is defined as follows [1]:

$$e_{\omega i} = k_{P\omega}(\omega_{ref} - \bar{\omega}) + k_{I\omega} \int (\omega_{ref} - \bar{\omega}) dt$$

$$\bar{\omega} = \frac{\sum_{i=1}^{N} \omega_i}{N}$$

$e_{\omega i}$ is the control signal used to restore the frequency of the DG to the reference frequency, ω_{ref}. The secondary voltage controller restores the voltage of the DG to the reference value, v_{ref}, using PI control of the error between the reference

and the average of the values, $\bar{v}$. The same method is used for the secondary frequency controller, with different PI controller gain values, k_{Pv} and k_{Iv}. As noted in [2], the line impedance effect limits the accuracy of reactive power sharing as voltage is not common throughout the microgrid. This reference [1] proposes a line-impedance-independent power equalization by implementing local secondary control for reactive power sharing thus a new control signal, e_{Qi}, is introduced in the secondary control and compares reactive power of each DG to the average reactive power for all DGs which acts as the reference.

The distributed averaging PI (DAPI) controller proposed in [10] requires communication between neighboring DGs in such a way that all DGs are connected to ensure power sharing. The DAPI frequency and voltage controllers are defined below, respectively [10]:

$$k_{\omega i}\dot{u}_{\omega,i} = -(\omega_i - \omega_{ref}) - \sum_{j=1}^{N} a_{ij}(u_{\omega,i} - u_{\omega,j})$$

$$k_{vi}\dot{u}_{v,i} = -\beta_i(v_i - v_{ref}) - \sum_{j=1}^{N} b_{ij}\left(\frac{Q_i}{Q_i^*} - \frac{Q_j}{Q_j^*}\right)$$

The compensation terms $u_{\omega,i}$ and $u_{v,i}$ are used as additional inputs to the standard droop equations in the primary control layer. The adjacency matrices are defined as a_{ij} and b_{ij} and the rated reactive power of the i^{th} DG is Q_i^*. It is important to recall that the line impedance effect creates a challenge for reactive power sharing. A tunable compromise between voltage regulation and reactive power sharing is presented here.

2.3 Discussion of Literature

In summary, the primary droop controllers are well known and widely accepted. The droop controllers take a secondary control input to realize accurate power sharing in the microgrid and stability of frequency and voltage output signals. As a generalization for distributed secondary control, the frequency and

voltage values of the i^{th} DG are compared to the values communicated by its neighboring DGs and to the reference value so that the frequency and voltage synchronize to their nominal values. Frequency is the same in each DG throughout the microgrid, so active power sharing can be maintained. Voltages, however, are not common throughout the MG, so reactive power sharing is not accurately maintained by the Q-V droop method. References [1, 2, 3, 10] note that simultaneous control of voltage and reactive power sharing is only possible in symmetric systems due to the line impedance effect so there must be a trade off. Reference [1] proposes to implement secondary control for power sharing locally and independently from voltage sensing mismatches to combat this problem. The algorithm proposed in [10] also accounts for this issue and presents a tunable compromise between the two objectives. The distributed control structure is more favorable than the centralized control structure due to its improved resilience thus, many methods for distributed secondary control have been developed. The following chapter will discuss the microgrid test system which will be used to analyze a distributed secondary control method.

CHAPTER 3

Problem Setting

In this chapter, I will describe the model that the secondary control algorithm will be applied to. First, the system configuration of the five DG microgrid is defined. This includes physical descriptions of each DG, filters, and their connecting branches. Renewable energy sources including solar, wind and hydro produce dc power and are the primary energy sources in microgrids. An inverter-based DG contains the dc power source and an inverter bridge to convert dc to ac power. Then parameter measurements, calculations, and local controller characteristics are presented to describe the dynamics of the microgrid model. The localised power, voltage, and current control loops adjust the frequency and voltage of the inverter. The DG is nonlinear by nature, so the direct quadrature (d-q) reference frame, rotating at the angular frequency of the DG dictated by primary control [3], is used to produce voltage and current components as inputs for the linear control loops. Finally, the communication network that is required for distributed secondary control of a microgrid is explained.

3.1 System Configuration

The distributed dc power sources of each DG connects to the microgrid via a pulse-width modulated voltage source inverter [23], LC filter, and lines connecting buses modelled as RL branches as shown in Figure 3. The transmission lines connecting each bus are modeled as series RL branches [3] with loads corresponding to each DG. The output voltages of each DG are measured at the v_o buses. This three-phase voltage measurement at each DG is used to calculate the parameters communicated in the secondary control layer: frequency, angular position of the rotating frame, power, and d-q components of the output voltage. The line-line

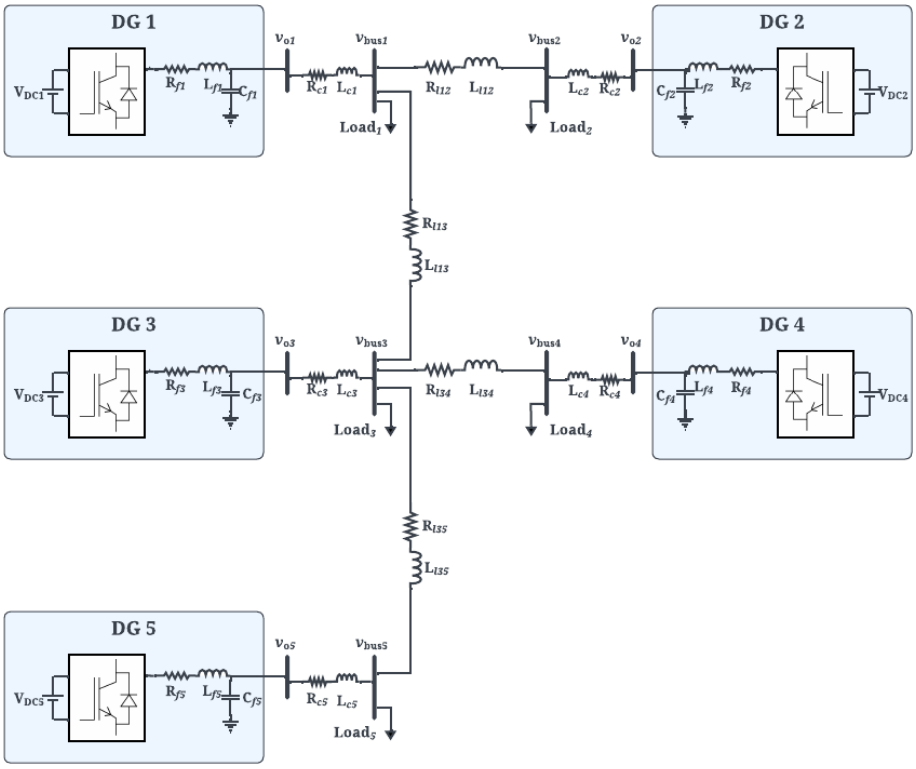

Figure 3. Diagram of the physical microgrid system [2, 3]

voltage of each DG is also measured here. At v_{bus} for each DG, frequency is measured. The line-line voltage and frequency at v_{bus} and the power measured at v_o are the parameters presented in the results section of this chapter.

3.2 Model Dynamics

The dc source generated by a renewable energy source or energy storage device is connected to the 3 arm inverter to convert dc power to ac power. The gate input signal of the inverter is dictated by the local power, voltage, and current controllers shown in Figure 4. The measured three phase output voltage and current signals of the DG are transformed by using a Park transformation to produce a dq0 rotating

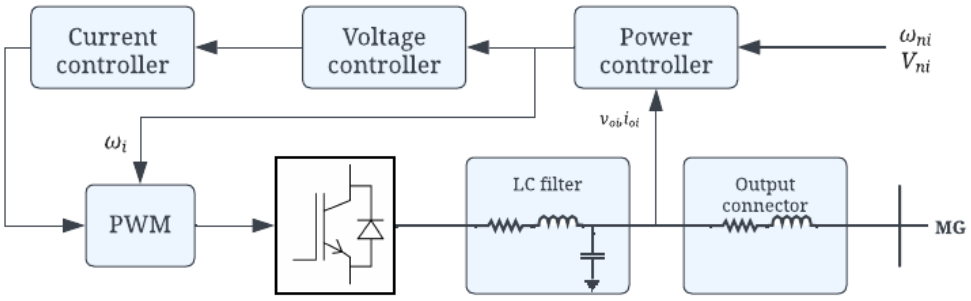

Figure 4. Block diagram of the control of one inverter-based DG [3, 4]

reference frame as documented in [24]:

$$V_d = \frac{2}{3}\left(V_a \sin(\omega t) + V_b \sin(\omega t - 2\pi/3) + V_c \sin(\omega t + 2\pi/3)\right)$$

$$V_q = \frac{2}{3}\left(V_a \cos(\omega t) + V_b \cos(\omega t - 2\pi/3) + V_c \cos(\omega t + 2\pi/3)\right)$$

$$V_0 = \frac{1}{3}\left(V_a + V_b + V_c\right)$$

where the input angular position used in the Park transformation, ωt, is the angle of measured frequency of the DG. The frequency and angular position are measured using a conventional phase-locked loop (PLL) [25]. The PLL takes the measured three-phase voltage at the output bus of the DG and uses a PI controller to calculate frequency and angular position. The angular position of the dq rotating reference frame, ω_i, used to calculate the current controller references and the inverter three-phase reference is calculated in the power controller. The power controller characteristics are shown in Figure 5. The output voltage and current measurements from the DG are transformed to the d-q components, v_{odi}, v_{oqi}, i_{odi} and i_{oqi}. The power controller then calculates the output active and reactive powers of the DG from the voltage and current signals. The secondary control outputs, ω_{ni} and V_{ni}, are used as inputs to the widely accepted droop control equations with droop coefficients m_i and n_i, based on the ratings of the DG to ensure balanced

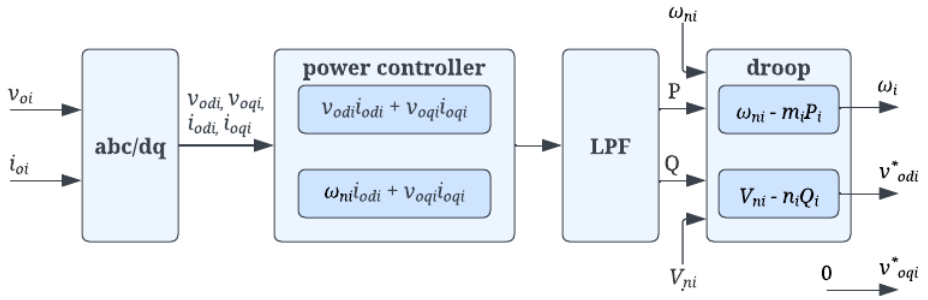

Figure 5. Block diagram of the power controller [3]

power sharing. The reference frequency and voltage values ω_i, v^*odi, and v^*_{oqi} are calculated by the droop control. The output reference voltage is aligned along the d-axis, so the q component is 0 [3].

The output voltage signals from the power controller are the references for the voltage controller. These are compared with the d-q components of the measured output voltages of the DG and passed through PI controllers as shown in Figure 6. The output values from the current controller and the operating frequency from the droop equation are used to control the inverter.

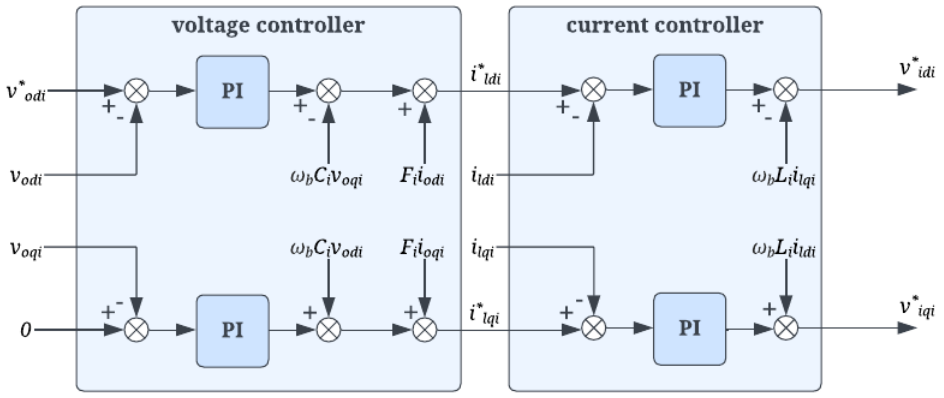

Figure 6. Block diagram of the voltage and current controllers [3]

3.3 Communication Topology

The distributed secondary control requires information exchange between neighboring DGs. Communication matrices are defined to designate which DGs are communicating. A 5-bus microgrid will be modeled so that there are five DGs and five corresponding loads. This model will be used to apply primary and secondary control algorithms to analyze their performance and their resilience against cyber threats and communication topology changes. Previously defined centralized controllers result in an inefficient and non robust system when sources are geographically dispersed and thus are not practical [26]. Considerations of distance between DGs and number of communication links can be used to define the communication digraph which may differ from the physical connection graph [10, 20, 27]. The chosen communication topology for the five DG microgrid used in this thesis is shown in Figure 7.

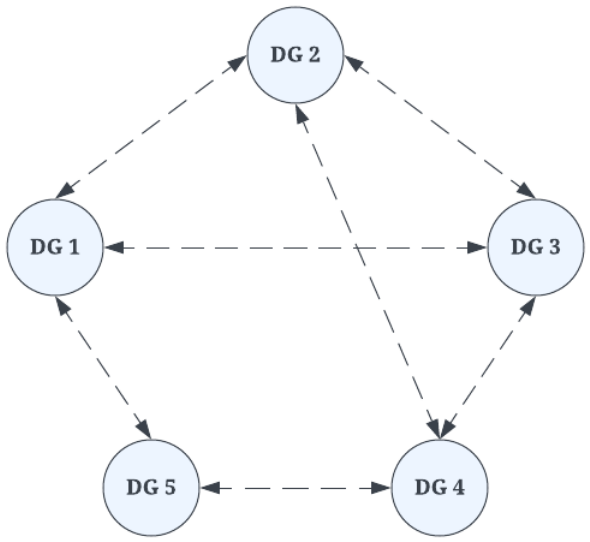

Figure 7. Communication digraph

The communication network is modeled as a digraph $G(V, E, A)$ where $V = \{1, ..., n\}$ is a nonempty set of labeled nodes, $E \subset V \times V$ is the set of edges or com-

munication links, and $A = [a_{ij}] \in R^{N \times N}$ is the weighted adjacency matrix. Each DG represents a node and if node i sends information to node j then $(i, j) \in E$ and $a_{ij} > 0$. The system configuration, model dynamics, and communication topology described in this chapter specify the microgrid model which a distributed secondary control method will be applied to. The following chapter will provide analysis of the hierarchical control of the microgrid model and threats to the system.

CHAPTER 4

Methodology

The required communication network for the secondary control of a microgrid creates vulnerabilities for cyber-physical threats such as denial of service (DOS), false data injection (FDI), and communication topology changes. It is important to test and analyze the response of the secondary control algorithm in the face of disturbance and cyber threats in order to verify performance and resilience.

4.1 Distributed Secondary Control

Secondary control is responsible for synchronization of voltage and frequency to their nominal values by exchanging information. In this thesis, I will focus on distributed cooperative control using feedback linearization proposed in [3] for a microgrid with nonlinear or non identical dynamics. Each DG in the microgrid is considered an agent in a networked multi-agent system where the secondary control is a tracking synchronization problem. Since the model dynamics are nonlinear and non identical, feedback linearization is adopted from [3] to transform the dynamics of the DGs to a linear model. The algorithm will be tested under conditions where there will be cyber threats, communication disruptions, and load changes to test resilience.

The primary droop control equations are as follows:

$$\omega_i = \omega_{ni} - m_i P_i$$

$$v^*_{o,magi} = V_{ni} - n_i Q_i$$

where $v^*_{o,magi}$ is the reference value for the voltage controller and is aligned along the d-axis so that the q component is 0. ω_{ni} and V_{ni} are the references defined in the secondary control layer. P_i and Q_i are the measured output power

values of DG_i. m_i and n_i are the droop coefficients chosen based on the power ratings of the DGs.

The secondary control equations follow $\mathbf{e}_i = \sum_{j \in N} a_{ij}(\mathbf{y}_i - \mathbf{y}_j) + g_i(\mathbf{y}_i - \mathbf{y}_0)$. In [3], only voltage control is defined using this equation, but it can be expanded for frequency control as well. Secondary voltage control defines V_{ni} such that the output voltage $v_{o,magi}$ approaches the nominal value v_{ref} in finite time. References [2, 3] state that the q-component of the output voltage is zero and $v_{o,magi} = \sqrt{v_{odi}^2 + v_{oqi}^2}$, so the sufficient condition for synchronization is satisfied such that $v_{odi} \to v_{ref}$. Thus, the secondary control equation can be defined as follows:

$$e_{vi} = \sum_{j \in N} a_{ij}(v_{odi} - v_{odj}) + g_i(v_{odi} - v_{ref})$$

$$V_{ni} = -k_v \int e_{vi} dt, i = 1, 2, ..., N$$

To ensure frequency synchronization, accurate active power sharing must also be considered. To achieve this, the following must be true:

$$\frac{P_i}{P_j} = \frac{m_j}{m_i}$$

The secondary frequency control will guarantee active power sharing and define ω_{ni} such that $\omega_i \to \omega_{ref}$ in the following way:

$$e_{fi} = -k_f \left(\sum_{j \in N} a_{ij}(\omega_i - \omega_j) + g_i(\omega_i - \omega_{ref}) \right) - k_p \sum_{j \in N} a_{ij}(m_i P_i - m_j P_j)$$

$$\omega_{ni} = \int e_{fi} dt, i = 1, 2, ..., N$$

The adjacency matrix of the digraph in Figure 7 is defined as:

$$A = \begin{bmatrix} 0 & 1 & 1 & 0 & 1 \\ 1 & 0 & 1 & 1 & 0 \\ 1 & 1 & 0 & 1 & 0 \\ 0 & 1 & 1 & 0 & 1 \\ 1 & 0 & 0 & 1 & 0 \end{bmatrix}$$

This adjacency matrix is used in the secondary control equations to define which DGs are communicating with each other. It is noted that the communication network defined in this thesis is bidirectional thus $a_{ij} = a_{ji}$.

4.2 Threat Models

Cyber-physical threats such as DOS, FDI, and communication disruptions will be modelled and applied to the microgrid. The secondary control should be able to continue to regulate frequency and voltage to nominal values for microgrid resilience.

4.2.1 Denial of Service

A DOS attack interrupts access to information communicated between DGs. The communicated data is blocked, or set to zero, for a specified time each period. For a defined time within the period, the communication link is set to zero and the information being exchanged is compromised. The DOS attack as it relates to the secondary control parameters can be characterized as follows:

$$\omega_i^j = \omega_i \times \Delta$$

$$v_{odi}^j = v_{odi} \times \Delta$$

$\Delta = \{0, 1\}$ is defined by the pulse width generator where 0 indicates the DOS attack and 1 indicates no attack. ω_i^j and v_{odi}^j indicate the information from the i^{th} DG communicated to the j^{th} DG.

In this thesis, the DOS attack will be modelled in two ways: a node-based attack and a link-based attack. As described in [4], the node-based attack will block all information exchange from one DG. In this thesis, DG 2 will be attacked hence DGs 1, 3, & 4, following Figure 7, will not receive information from DG 2 nor will DG 2 receive information from any neighboring DGs while under attack. The link-based attack blocks information from being communicated across a specified

link between DGs. Here, the link-based DOS attack will interrupt information exchange between DGs 2 & 3.

4.2.2 False Data Injection

Data is falsified at frequency communication links in the secondary control layer to model an FDI attack. This affects the integrity of the information being exchanged between DGs. The corrupted data from the FDI being communicated between DGs is modelled by [12]:

$$\omega_i^j = \omega_i + \omega_i^a$$

The disturbance added to falsify communicated frequency measurements from the i^{th} DG is defined as ω_i^a . Thus, $\omega_i^a = 0$ indicates that the communicated data remains unaffected. The FDI attack modelled in this thesis targets information shared on a communication link. In the link-based attack, the controller of one DG will receive corrupted frequency values from the neighboring DG on the targeted link [28]. In this case, the link between DGs 2 & 3 is compromised so DG 2 will receive corrupted data from DG 3 and vice versa. All other communication links to and from those DGs are unaffected.

4.2.3 Communication Disruption

This thesis will investigate the microgrid's response to changes in the communication network. The communication digraph shown in Figure 7 of the microgrid is defined by the adjacency matrix. Thus, the secondary controller equations are directly affected by changes in the communication network. Communication disruptions in the microgrid are modelled by removing the connection between several DGs thus changing the topology of the communication network. The resilience of the microgrid is then analyzed by examining the frequency, power, and voltage of each DG in response to load changes following the communication disruption. The

adjacency matrix will be altered such that the links between DGs 2 & 4, 1 & 3, and 1 & 5 are disrupted:

$$A = \begin{bmatrix} 0 & 1 & 0 & 0 & 0 \\ 1 & 0 & 0 & 0 & 0 \\ 0 & 1 & 0 & 1 & 0 \\ 0 & 0 & 1 & 0 & 1 \\ 0 & 0 & 0 & 1 & 0 \end{bmatrix}$$

The altered adjacency matrix sets $a_{24} = a_{13} = a_{15} = 0$. Hence, the communication digraph becomes sparse while still maintaining a spanning tree, meaning there is a direct path from one DG to every other DG in the microgrid [3]. The disrupted communication digraph is shown below:

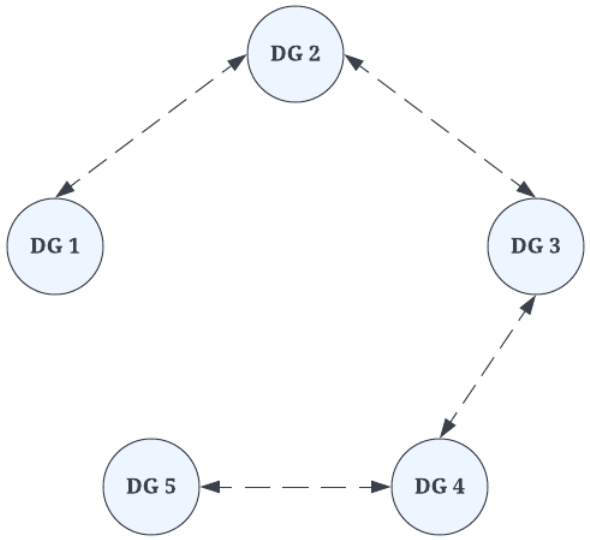

Figure 8. Communication digraph after communication disruption

CHAPTER 5

Simulation and Analysis

5.1 Simulation Environment

All modelling and data collection was completed in the MATLAB/Simulink environment. MATLAB is a numeric computing platform typically used to model, analyze data, and develop algorithms. Simscape Electrical, developed for modeling power systems in Simulink, provides components for applications such as smart grids and renewable energy systems which can be used to analyze the generation, conversion, transmission, and consumption of electrical power at the grid level. Simscape supports C-code generation, giving the capability to be used in hardware-in-the-loop systems for further testing.

5.2 System Specifications

The nominal voltage and frequency values of the microgrid are 380V and 50Hz, respectively [19]. The voltage and frequency references are derived as follows:

$$V_{ref} = \frac{V_{L-L}\sqrt{2}}{\sqrt{3}}$$

$$\omega_{ref} = f \times 2\pi$$

The load at each DG is defined as: $load_1 = load_4 = 30kW$ and $load_2 = load_3 = load_5 = 20kW$. Thus, the total load of the microgrid is 120kW. The total active load on the system must equal the total active power generation of each DG to balance generation and load [29] as such:

$$\sum_{i \in N} load_i = \sum_{i \in N} P_i$$

As adopted from [3], the droop coefficients used in the primary control layer and the PI controller coefficients used in the local voltage and current controllers are listed in Table 1.

Table 1. Microgrid Specifications

Parameter	**DGs 1, 3, & 5**	**DGs 2 & 4**
m	9.4×10^{-5}	12.5×10^{-5}
n	1.3×10^{-3}	1.5×10^{-3}
K_{PV}	0.1	0.05
K_{IV}	420	390
K_{PC}	15	10.5
K_{IC}	2×10^4	1.6×10^4
R_f	0.1Ω	
L_f	1.35mH	
C_f	50μF	
R_c	0.03Ω	
L_c	0.35mH	
R_l	0.23Ω	
L_l	318μH	
ω_b	100π rad	

In Table 2, the secondary control parameters are listed. Reference values for secondary frequency and voltage control are ω_{ref} and v_{ref}, respectively. In this thesis, every DG will have access to the reference value, so all pinning gains are defined as follows: $g_1 = g_2 = g_3 = g_4 = g_5 = 1$. The secondary control voltage, power, and frequency gains are also listed in Table 2.

Table 2. Secondary Control Parameters

Parameter	**Value**
ω_{ref}	100π rad
v_{ref}	310.27 V
k_v	10
k_p	10
k_f	18

5.3 Results

Each case study for simulation will be described and the results will be presented in the remainder of this chapter. Each simulation of the microgrid will include a load change of each DG at t=1s and a load change of DG 2 at t=5s and t=8s to thoroughly compare results. At t=1s the loads of each DG will increase to the following values: $load_1 = load_4 = 45kW$ and $load_2 = load_3 = load_5 = 40kW$. The resulting total load of the system after this load change is 210kW. The load at DG 2 will increase to $load_2 = 50kW$ at t=5s and decrease back to $load_2 = 40kW$ at t=8s. To be able to compare frequency and voltage regulation and active power sharing while employing distributed cooperative secondary control in the microgrid, a baseline simulation is used. The baseline results are shown in Figure 9. These results indicate slight oscillations at each load change, but frequency and voltage become stable and regulate to the nominal values, 50Hz and 380V, respectively. The active power values of each DG indicate that the microgrid maintains active power sharing, and the signals become stable after minor oscillations at each load change. The total active power generated throughout the simulation is equal to the total demand on the system. The following case studies describe the response this system has to the previously described threat models including DOS attack, FDI attack, and communication disruption.

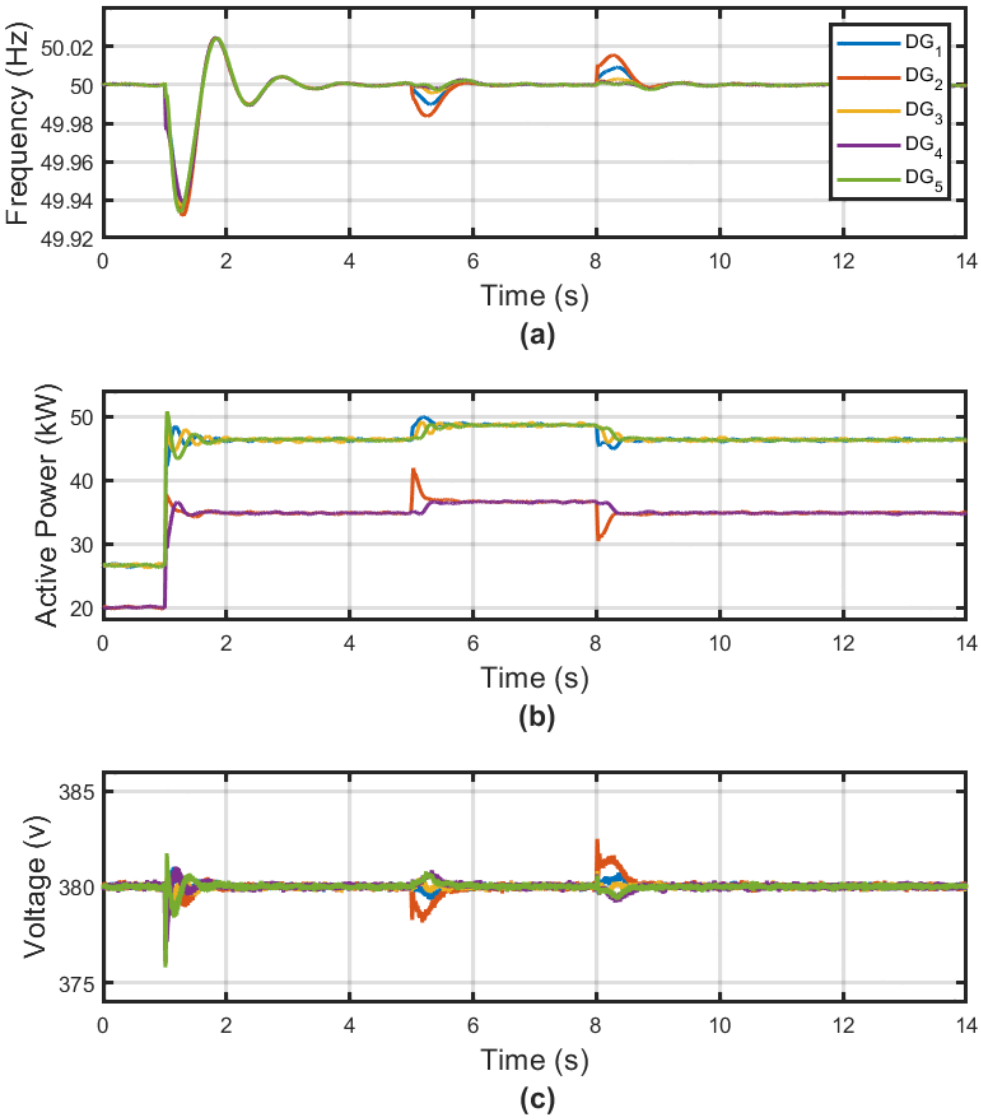

Figure 9. Baseline microgrid simulation results: (a) Frequency, (b) Power, and (c) Voltage of each DG.

5.3.1 Case Study for DOS Attack

In this thesis, the DOS attack is modelled in two ways. One attack model targets a node, or a DG. The other DOS attack model targets a link between DGs. In both cases, the DOS model is effectively altering the communication networks of the microgrid through these attacks. Figures 10 and 11 illustrate the impact

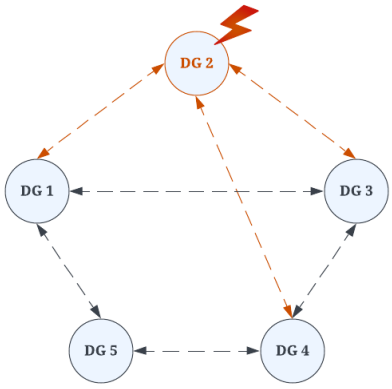

Figure 10. Communication topology under DOS node-based attack

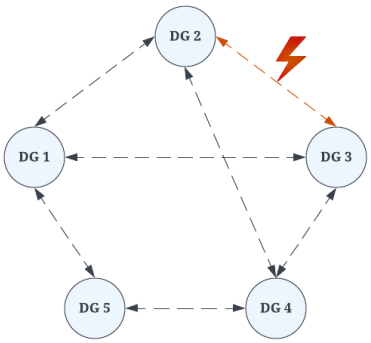

Figure 11. Communication topology under DOS link-based attack

of the node-based DOS attack and link-based DOS attack, respectively, on the communication topology of the microgrid. Targeting the node at DG 2 affects the communication links between DG 2 and DGs 1, 3, & 4. Attacking the link between DGs 2 & 3 will only impact the communicated information between those two DGs.

The distributed cooperative secondary control should be able to stabilize and regulate frequency and voltage as well as maintain active power sharing against a DOS attack. Figure 12 shows the response of each DG while under the node-based DOS attack on DG 2. Compared to the baseline results, the control algorithm is capable of stabilizing frequency and voltage in finite time despite increased oscillation and peak values. The active power of each DG does not experience

significant oscillation. The results of the link-based DOS attack are shown in Figure 13. Although we can observe slight oscillations at each load change, they do not differ significantly from those of the baseline model. This is to be expected since the microgrid still maintains spanning tree, meaning all DGs have a direct path to one another through the communication network. Despite the attack on the communication link between DGs 2 & 3, the system remains stable and resilient.

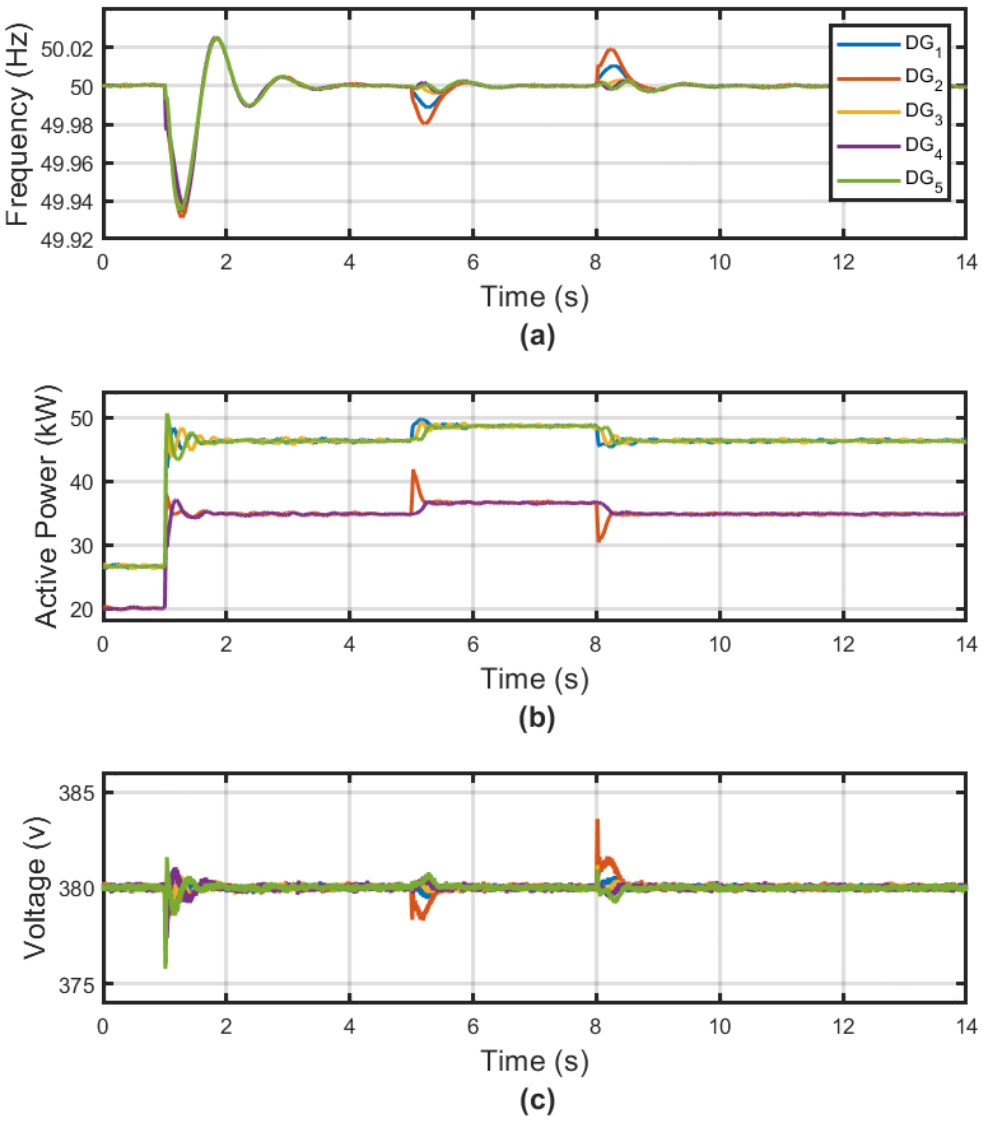

Figure 12. Microgrid simulation results under DOS node-based attack: (a) Frequency, (b) Power, and (c) Voltage of each DG.

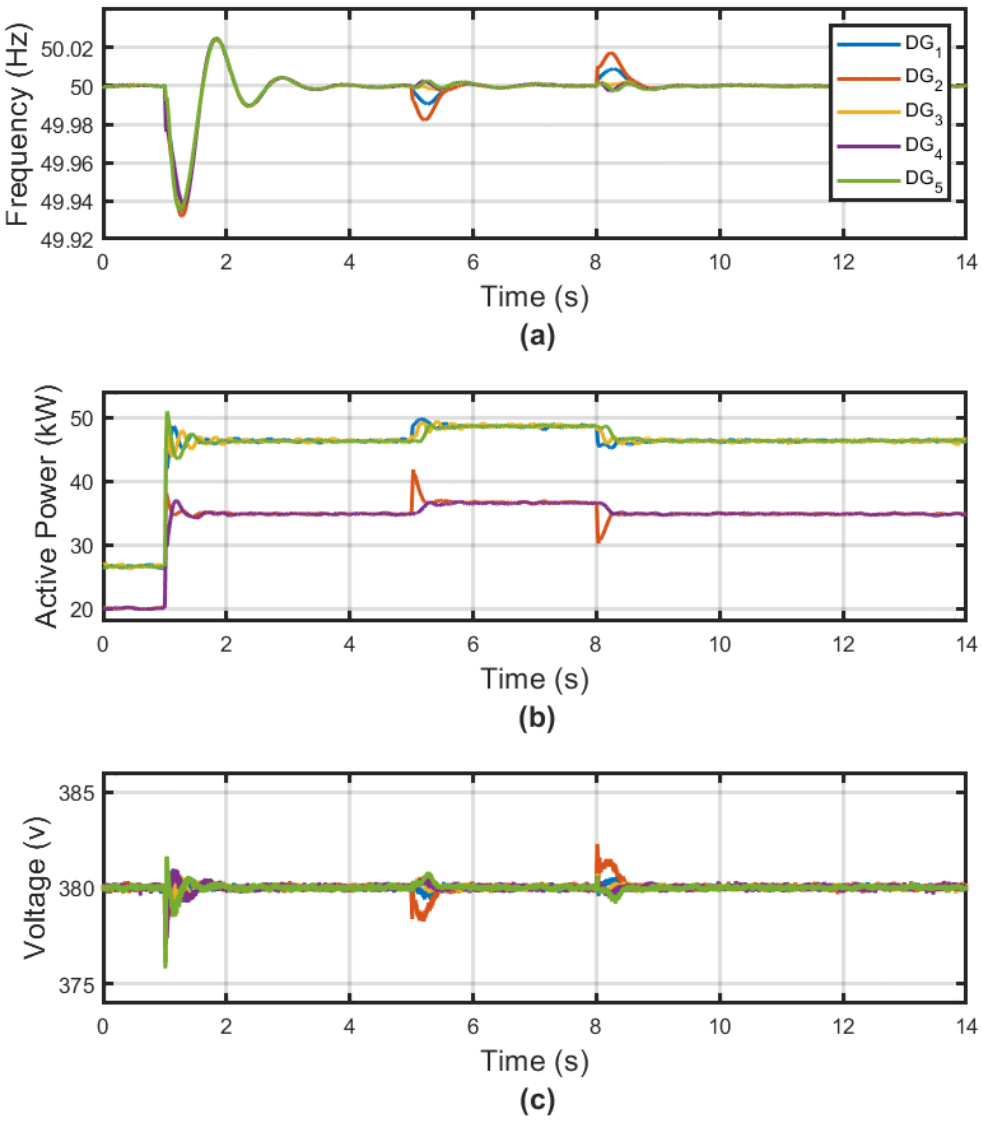

Figure 13. Microgrid simulation results under DOS link-based attack: (a) Frequency, (b) Power, and (c) Voltage of each DG.

5.3.2 Case Study for FDI Attack

The FDI attack modelled in this thesis corrupts frequency information being sent on the communication link between DGs 2 & 3. One case is considered where the attack signal is defined as $\omega_i^a \sim U[-2, 2]$Hz. The results are shown in Figure 14. This FDI attack affects the microgrid such that the frequency, active power, and voltage experience some oscillation, but the system remains stable nonetheless. The oscillation in the frequency of each DG in particular is noteworthy. Figure 14 (a) shows that the frequency of DG 2 has a higher peak oscillation compared to the baseline model. Similarly, a second case is considered where $\omega_i^a \sim U[-5, 5]$Hz, as shown in Figure 15. In this case, the oscillations are more prominent. Frequency, active power, and voltage all experience oscillations with greater peaks compared to the base model and the FDI attack with a 2Hz data injection. Despite this, the frequency and voltage still stabilize and regulate to the nominal values of 50Hz and 380V. The frequency oscillations remain within a $\pm$0.02Hz bound of the nominal frequency.

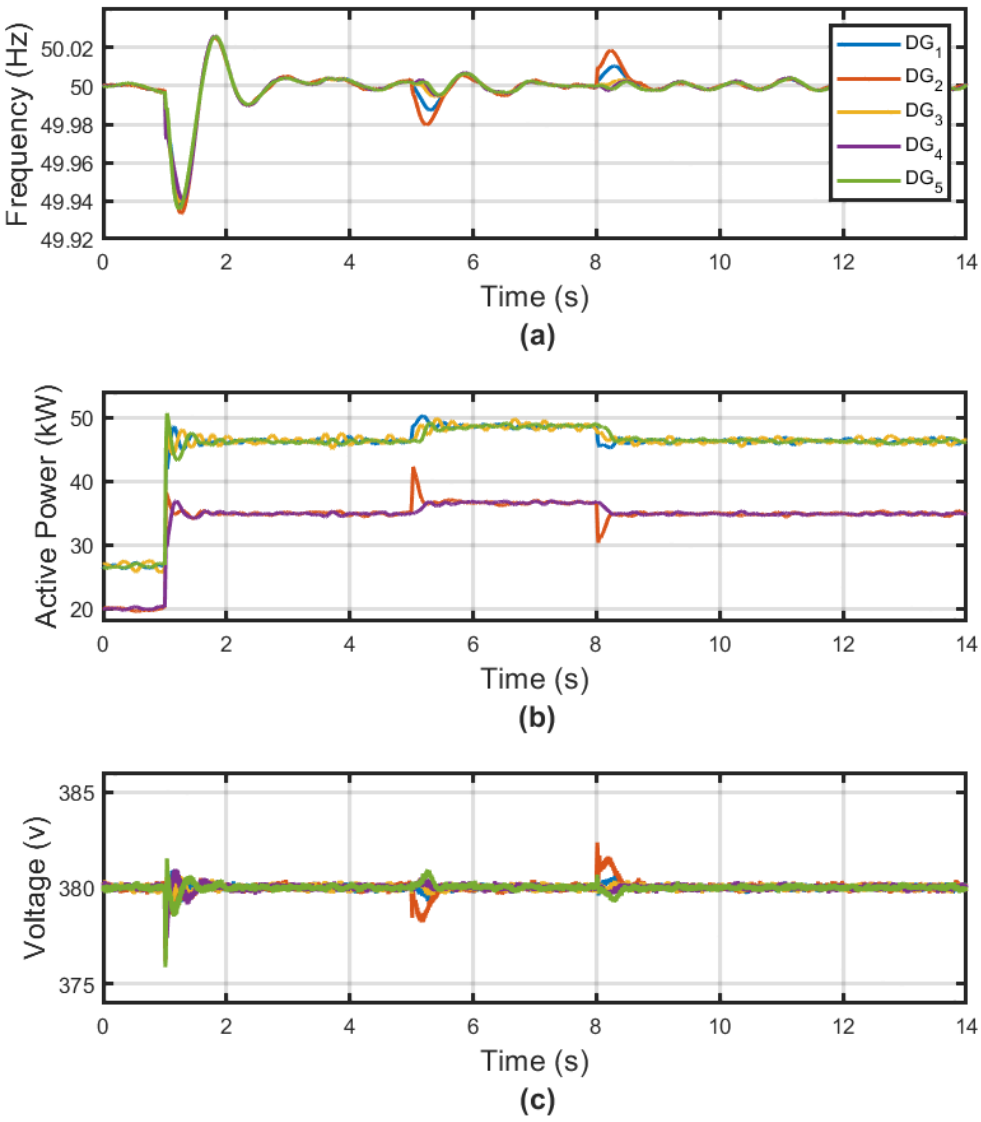

Figure 14. Microgrid simulation results under FDI attack with 2Hz data injection: (a) Frequency, (b) Power, and (c) Voltage of each DG.

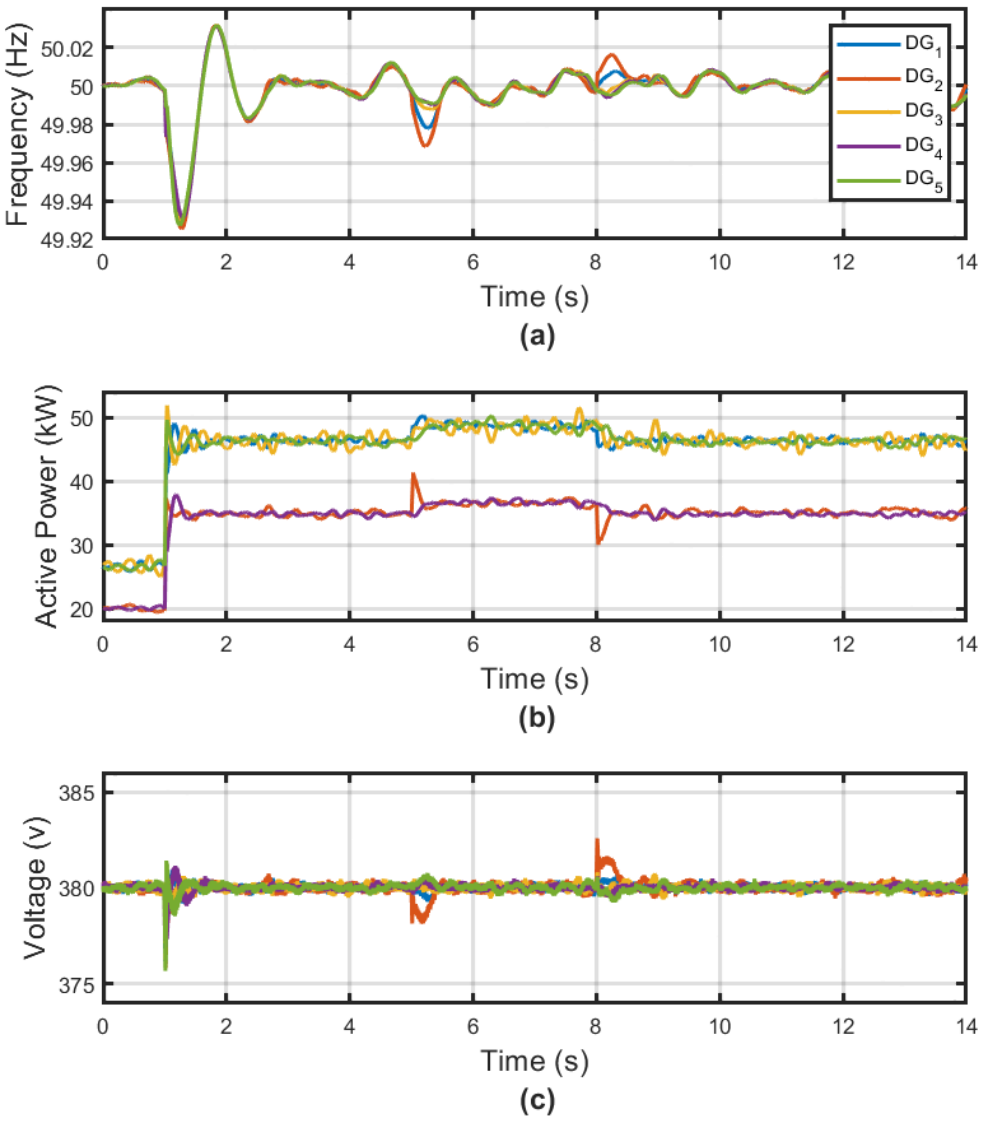

Figure 15. Microgrid simulation results under FDI attack with 5Hz data injection: (a) Frequency, (b) Power, and (c) Voltage of each DG.

5.3.3 Case Study for Communication Disruption

The communication links between DGs 1 & 3, 1 & 5, and 2 & 4 are disrupted at t=3s, which results in the communication graph as shown in Figure 8 in Chapter 4. The results of this communication disruption in Figure 16 indicate that the control algorithm still maintains stability, regulation, and power sharing despite changes in the communication network. This much more sparse network results in slower convergence times compared to the base model which is not ideal, but it is acceptable and proves the system is adaptable and thus resilient.

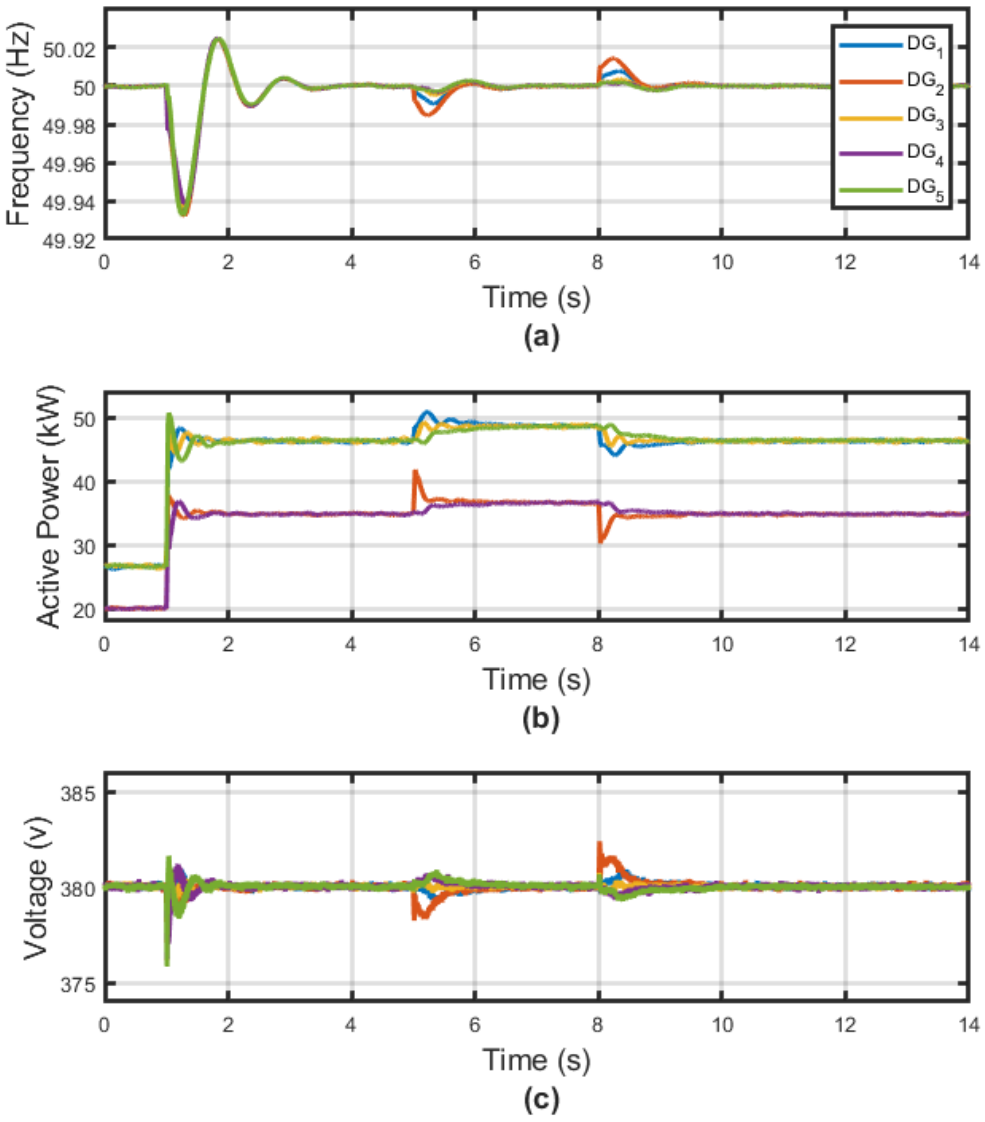

Figure 16. Microgrid simulation results under communication disruption: (a) Frequency, (b) Power, and (c) Voltage of each DG.

CHAPTER 6

Conclusion and Future Work

Negative impacts on the environment that are primarily caused by burning fossil fuels and CO_2 emissions can be attributed to conventional power generation and increasing electricity usage. Additionally, electric power demand is rising due to rising popularity of electric vehicles and other electric applications. An increasingly popular solution for these problems is to integrate renewable energy sources to our existing power grid. A favorable method of making this possible is the deployment of microgrids, low voltage distributed systems consisting of generators, loads, and storage devices.

When a microgrid is not connected to the main power grid, it must regulate and stabilize frequency and voltage values using control techniques. Primary control stabilizes frequency and voltage which may result in deviations from nominal values. Thus, secondary control is required to account for these deviations. Primary droop control methods are widely accepted and have been proven to be sufficient in maintaining stability. However, there have been many studies on secondary control algorithms. The most notable discovery being that distributed control proves more resilient than centralized control methods.

The central control structure requires a complex control network, as opposed to distributed control with a more sparse network and improved reliability. Therefore, many distributed secondary control methods have been developed over past decades, which demonstrated their effectiveness and advantages. On the other hand, distributed microgrids are vulnerable to possible cyber threats because of the required networked communication between neighboring DGs. Thus, microgrids must prove resilient to such attacks as well as other possible disturbances.

To address these challenges, in this thesis, Matlab Simulink is used to analyze secondary control for maintaining frequency and voltage stability against cyber threats, load changes, and communication topology changes between DGs. Specifically, in this thesis I focused on three types of cyber threats, including DOS attack which denies access to communicated information, FDI attack that alters the integrity of data, and communication disruption which changes the communication topology of the microgrid.

In terms of research method, distributed cooperative control adopted in part from [3] was applied to a microgrid's secondary control layer to test its resilience against various threats or disturbances. In each case study examining the microgrid's response to the three threats modelled in this thesis, the secondary control algorithm is able to stabilize frequency and voltage, regulate them to their nominal values, and maintain active power sharing. Numerous simulations with a five DG microgrid demonstrate that the secondary control method can enable the microgrid to adapt to load changes while under threat and maintain balance between generation and load under the aforementioned three types of cyber threats and disruptions.

To further examine the effect of secondary control on the resilience of microgrids, there are several interesting future research directions. For instance, the system remains stable if there is no load change or disturbance. In order to examine the response of the microgrid under threat, load changes were implemented to disturb the system and analyze the response and convergence of output signals to nominal values. In a real world application, loads are typically not constant and are always varying. The next step for this research is to apply secondary control to a more dynamic system with variable loads which are constantly changing to analyze the stability of the system. Secondly, varying the physical and cyber topol-

ogy of the microgrid is a future research consideration. Scaling up the microgrid presents new challenges when designing the communication topologies. Optimizing the communication network becomes more complicated when considering cyber threats, economics, and computational cost. There must be a balance between the sparseness of the communication network and maintaining spanning tree and resilience under cyber attacks that threaten communication links. When speaking about likelihood of threats occurring on communication links and of losing spanning tree, machine learning methods may be considered as well. These methods may be used to optimize the communication topology as well as prescribe weighted communication links to further improve resilience. Lastly, machine learning methods may be used to classify faults or disturbances within the system to improve the response a microgrid has to such a disturbance. In the case of the false data injection attack, for example, the output signals experienced increased oscillation throughout the duration of the attack. A machine learning algorithm may be able to identify this type of threat and the system would be better suited to pinpoint the source of the disturbance. All of these are interesting and promising future research directions along this topic.

LIST OF REFERENCES

[1] Q. Shafiee, J. M. Guerrero, and J. C. Vasquez, "Distributed secondary control for islanded microgrids—a novel approach," *IEEE Transactions on Power Electronics*, vol. 29, no. 2, pp. 1018–1031, 2014.

[2] N. M. Dehkordi, N. Sadati, and M. Hamzeh, "Distributed robust finite-time secondary voltage and frequency control of islanded microgrids," *IEEE Transactions on Power Systems*, vol. 32, no. 5, pp. 3648–3659, 2017.

[3] A. Bidram, A. Davoudi, F. L. Lewis, and J. M. Guerrero, "Distributed cooperative secondary control of microgrids using feedback linearization," *IEEE Transactions on Power Systems*, vol. 28, no. 3, pp. 3462–3470, 2013.

[4] L. Ding, Q.-L. Han, B. Ning, and D. Yue, "Distributed resilient finite-time secondary control for heterogeneous battery energy storage systems under denial-of-service attacks," *IEEE Transactions on Industrial Informatics*, vol. 16, no. 7, pp. 4909–4919, 2020.

[5] United Nations. "Generating power." july 2020. [Online]. Available: https://www.un.org/en/climatechange/climate-solutions/cities-pollution

[6] US Department of Energy. "Building a better grid: Addressing climate change and bolstering electric grid security through planning & innovation." july 2022. [Online]. Available: https://www.energy.gov/policy/articles/building-better-grid-addressing-climate-change-and-bolstering-electric-grid

[7] International Energy Agency. "World energy outlook 2022." october 2022. [Online]. Available: https://www.iea.org/reports/world-energy-outlook-2022

[8] A. Bidram, A. Davoudi, and F. L. Lewis, "A multiobjective distributed control framework for islanded ac microgrids," *IEEE Transactions on Industrial Informatics*, vol. 10, no. 3, pp. 1785–1798, 2014.

[9] D. T. Ton and M. A. Smith, "The u.s. department of energy's microgrid initiative," *The Electricity Journal*, vol. 25, no. 8, pp. 84–94, 2012.

[10] J. W. Simpson-Porco, Q. Shafiee, F. Dörfler, J. C. Vasquez, J. M. Guerrero, and F. Bullo, "Secondary frequency and voltage control of islanded microgrids via distributed averaging," *IEEE Transactions on Industrial Electronics*, vol. 62, no. 11, pp. 7025–7038, 2015.

[11] Z. Lian, C. Deng, C. Wen, F. Guo, and P. L. sand Wentao Jiang, "Distributed event-triggered control for frequency restoration and active power allocation in microgrids with varying communication time delays," *IEEE Transactions on Industrial Electronics*, vol. 68, no. 9, pp. 8367–8378, 2021.

[12] Z. Shahbazi, A. Ahmadi, A. Karimi, and Q. SHafiee, "Performance and vulnerability of distributed secondary control of ac microgrids under cyber-attack," in *7th International Conference on Control, Instrumentation and Automation (ICCIA)*, 2021, pp. 1–6.

[13] S. Sahoo, Y. Yang, and F. Blaabjerg, "Resilient synchronization strategy for ac microgrids under cyber attacks," *IEEE Transactions on Power Electronics*, vol. 36, no. 1, pp. 73–77, 2021.

[14] H. Zhang, P. Cheng, L. Shi, and J. Chen, "Optimal dos attack policy against remote state estimation," in *52nd IEEE Conference on Decision and Control*, 2013, pp. 5444–5449.

[15] H. F. Habib, C. R. Lashway, and O. A. Mohammed, "A review of communication failure impacts on adaptive microgrid protection schemes and the use of energy storage as a contingency," *IEEE Transactions on Industry Applications*, vol. 54, no. 2, pp. 1194–1207, 2018.

[16] A. Bidram and A. Davoudi, "Hierarchical structure of microgrids control system," *IEEE Transactions on Smart Grid*, vol. 3, no. 4, pp. 1963–1976, 2012.

[17] Z. Miao, A. Domijan, and L. Fan, "Investigation of microgrids with both inverter interfaced and direct ac-connected distributed energy resources," *IEEE Transactions on Power Delivery*, vol. 26, no. 3, pp. 1634–1642, 2011.

[18] Q. Zhou, M. Shahidehpour, M. Yan, X. Wu, A. Alabdulwahab, and A. Abusorrah, "Distributed secondary control for islanded microgrids with mobile emergency resources," *IEEE Transactions on Power Systems*, vol. 35, no. 2, pp. 1389–1399, 2020.

[19] J. M. Guerrero, J. C. Vasquez, J. Matas, L. G. de Vicuna, and M. Castilla, "Hierarchical control of droop-controlled ac and dc microgrids—a general approach toward standardization," *IEEE Transactions on Industrial Electronics*, vol. 58, no. 1, pp. 158–172, 2011.

[20] F. Guo, C. Wen, J. Mao, and Y.-D. Song, "Distributed secondary voltage and frequency restoration control of droop-controlled inverter-based microgrids," *IEEE Transactions on Industrial Electronics*, vol. 62, no. 7, pp. 4355–4364, 2015.

[21] M. Shi, X. Chen, J. Zhou, Y. Chen, J. Wen, and H. He, "Pi-consensus based distributed control of ac microgrids," *IEEE Transactions on Power Systems*, vol. 35, no. 3, pp. 2268–2278, 2020.

[22] J. Lopes, C. Moreira, and A. Madureira, "Defining control strategies for microgrids islanded operation," *IEEE Transactions on Power Systems*, vol. 21, no. 2, pp. 916–924, 2006.

[23] Y. A.-R. I. Mohamed and A. A. Radwan, "Hierarchical control system for robust microgrid operation and seamless mode transfer in active distribution systems," *IEEE Transactions on Smart Grid*, vol. 2, no. 2, pp. 352–362, 2011.

[24] Mathworks. "abc to dq0, dq0 to abc." 2013. [Online]. Available: https://www.mathworks.com/help/sps/powersys/ref/abctodq0dq0toabc.html

[25] S. Golestan, J. M. Guerrero, and J. C. Vasquez, "Steady-state linear kalman filter-based plls for power applications: A second look," *IEEE Transactions on Industrial Electronics*, vol. 65, no. 12, pp. 9795–9800, 2018.

[26] H. Xin, Z. Qu, J. Seuss, and A. Maknouninejad, "A self-organizing strategy for power flow control of photovoltaic generators in a distribution network," *IEEE Transactions on Power Systems*, vol. 26, no. 3, pp. 1462–1473, 2011.

[27] C. Burgos-Mellado, J. J. Llanos, R. Cárdenas, D. Sáez, D. E. Olivares, M. Sumner, and A. Costabeber, "Distributed control strategy based on a consensus algorithm and on the conservative power theory for imbalance and harmonic sharing in 4-wire microgrids," *IEEE Transactions on Smart Grid*, vol. 11, no. 2, pp. 1604–1619, 2020.

[28] S. Abhinav, H. Modares, F. L. Lewis, F. Ferrese, and A. Davoudi, "Synchrony in networked microgrids under attacks," *IEEE Transactions on Smart Grid*, vol. 9, no. 6, pp. 6731–6741, 2018.

[29] Center for Climate and Energy Solutions. [Online]. Available: https://www.c2es.org/content/microgrids/

BIBLIOGRAPHY

Abhinav, S., Modares, H., Lewis, F. L., Ferrese, F., and Davoudi, A., "Synchrony in networked microgrids under attacks," *IEEE Transactions on Smart Grid*, vol. 9, no. 6, pp. 6731–6741, 2018.

Bidram, A. and Davoudi, A., "Hierarchical structure of microgrids control system," *IEEE Transactions on Smart Grid*, vol. 3, no. 4, pp. 1963–1976, 2012.

Bidram, A., Davoudi, A., and Lewis, F. L., "A multiobjective distributed control framework for islanded ac microgrids," *IEEE Transactions on Industrial Informatics*, vol. 10, no. 3, pp. 1785–1798, 2014.

Bidram, A., Davoudi, A., Lewis, F. L., and Guerrero, J. M., "Distributed cooperative secondary control of microgrids using feedback linearization," *IEEE Transactions on Power Systems*, vol. 28, no. 3, pp. 3462–3470, 2013.

Burgos-Mellado, C., Llanos, J. J., Cárdenas, R., Sáez, D., Olivares, D. E., Sumner, M., and Costabeber, A., "Distributed control strategy based on a consensus algorithm and on the conservative power theory for imbalance and harmonic sharing in 4-wire microgrids," *IEEE Transactions on Smart Grid*, vol. 11, no. 2, pp. 1604–1619, 2020.

Center for Climate and Energy Solutions. [Online]. Available: https://www.c2es.org/content/microgrids/

Dehkordi, N. M., Sadati, N., and Hamzeh, M., "Distributed robust finite-time secondary voltage and frequency control of islanded microgrids," *IEEE Transactions on Power Systems*, vol. 32, no. 5, pp. 3648–3659, 2017.

Ding, L., Han, Q.-L., Ning, B., and Yue, D., "Distributed resilient finite-time secondary control for heterogeneous battery energy storage systems under denial-of-service attacks," *IEEE Transactions on Industrial Informatics*, vol. 16, no. 7, pp. 4909–4919, 2020.

Golestan, S., Guerrero, J. M., and Vasquez, J. C., "Steady-state linear kalman filter-based plls for power applications: A second look," *IEEE Transactions on Industrial Electronics*, vol. 65, no. 12, pp. 9795–9800, 2018.

Guerrero, J. M., Vasquez, J. C., Matas, J., de Vicuna, L. G., and Castilla, M., "Hierarchical control of droop-controlled ac and dc microgrids—a general approach toward standardization," *IEEE Transactions on Industrial Electronics*, vol. 58, no. 1, pp. 158–172, 2011.

Guo, F., Wen, C., Mao, J., and Song, Y.-D., "Distributed secondary voltage and frequency restoration control of droop-controlled inverter-based microgrids," *IEEE Transactions on Industrial Electronics*, vol. 62, no. 7, pp. 4355–4364, 2015.

Habib, H. F., Lashway, C. R., and Mohammed, O. A., "A review of communication failure impacts on adaptive microgrid protection schemes and the use of energy storage as a contingency," *IEEE Transactions on Industry Applications*, vol. 54, no. 2, pp. 1194–1207, 2018.

Institute of Electrical and Electronics Engineers. [Online]. Available: ieee.org

International Energy Agency. "World energy outlook 2022." october 2022. [Online]. Available: https://www.iea.org/reports/world-energy-outlook-2022

Lian, Z., Deng, C., Wen, C., Guo, F., and sand Wentao Jiang, P. L., "Distributed event-triggered control for frequency restoration and active power allocation in microgrids with varying communication time delays," *IEEE Transactions on Industrial Electronics*, vol. 68, no. 9, pp. 8367–8378, 2021.

Lopes, J., Moreira, C., and Madureira, A., "Defining control strategies for microgrids islanded operation," *IEEE Transactions on Power Systems*, vol. 21, no. 2, pp. 916–924, 2006.

Mathworks. [Online]. Available: https://www.mathworks.com/products/simulink.html

Mathworks. "abc to dq0, dq0 to abc." 2013. [Online]. Available: https://www.mathworks.com/help/sps/powersys/ref/abctodq0dq0toabc.html

Miao, Z., Domijan, A., and Fan, L., "Investigation of microgrids with both inverter interfaced and direct ac-connected distributed energy resources," *IEEE Transactions on Power Delivery*, vol. 26, no. 3, pp. 1634–1642, 2011.

Mohamed, Y. A.-R. I. and Radwan, A. A., "Hierarchical control system for robust microgrid operation and seamless mode transfer in active distribution systems," *IEEE Transactions on Smart Grid*, vol. 2, no. 2, pp. 352–362, 2011.

Sahoo, S., Yang, Y., and Blaabjerg, F., "Resilient synchronization strategy for ac microgrids under cyber attacks," *IEEE Transactions on Power Electronics*, vol. 36, no. 1, pp. 73–77, 2021.

Shafiee, Q., Guerrero, J. M., and Vasquez, J. C., "Distributed secondary control for islanded microgrids—a novel approach," *IEEE Transactions on Power Electronics*, vol. 29, no. 2, pp. 1018–1031, 2014.

Shahbazi, Z., Ahmadi, A., Karimi, A., and SHafiee, Q., "Performance and vulnerability of distributed secondary control of ac microgrids under cyber-attack," in *7th International Conference on Control, Instrumentation and Automation (ICCIA)*, 2021, pp. 1–6.

Shi, M., Chen, X., Zhou, J., Chen, Y., Wen, J., and He, H., "Pi-consensus based distributed control of ac microgrids," *IEEE Transactions on Power Systems*, vol. 35, no. 3, pp. 2268–2278, 2020.

Simpson-Porco, J. W., Shafiee, Q., Dörfler, F., Vasquez, J. C., Guerrero, J. M., and Bullo, F., "Secondary frequency and voltage control of islanded microgrids via distributed averaging," *IEEE Transactions on Industrial Electronics*, vol. 62, no. 11, pp. 7025–7038, 2015.

Ton, D. T. and Smith, M. A., "The u.s. department of energy's microgrid initiative," *The Electricity Journal*, vol. 25, no. 8, pp. 84–94, 2012.

United Nations. "Generating power." july 2020. [Online]. Available: https://www.un.org/en/climatechange/climate-solutions/cities-pollution

US Department of Energy. "Building a better grid: Addressing climate change and bolstering electric grid security through planning & innovation." july 2022. [Online]. Available: https://www.energy.gov/policy/articles/building-better-grid-addressing-climate-change-and-bolstering-electric-grid

Xin, H., Qu, Z., Seuss, J., and Maknouninejad, A., "A self-organizing strategy for power flow control of photovoltaic generators in a distribution network," *IEEE Transactions on Power Systems*, vol. 26, no. 3, pp. 1462–1473, 2011.

Zhang, H., Cheng, P., Shi, L., and Chen, J., "Optimal dos attack policy against remote state estimation," in *52nd IEEE Conference on Decision and Control*, 2013, pp. 5444–5449.

Zhou, Q., Shahidehpour, M., Yan, M., Wu, X., Alabdulwahab, A., and Abusorrah, A., "Distributed secondary control for islanded microgrids with mobile emergency resources," *IEEE Transactions on Power Systems*, vol. 35, no. 2, pp. 1389–1399, 2020.